Chemical looping combustion of petcoke using two natural ores in a 10 KW_{th} continuous pilot plant: a performance comparison

Nicolas Vin*, Kristina Bakoc, Arnold Lambert, William Pelletant, Stéphane Bertholin

IFP Energies nouvelles Rond-point de l'échangeur de Solaize BP 3, 69360 Solaize, France

ABSTRACT: Chemical looping combustion (CLC) technology has emerged as one of the most important clean fossil fuel combustion technologies, as it allows for sequestration of CO_2 with minimal increase in energy requirements and fuel demand in comparison to traditional plants. In the framework of the CHEERS project, the core technology of CLC process is being developed into a 3 MW_{th} system prototype for demonstration in an operational environment using petcoke as fuel. One of the main objectives is the selection of the oxygen carrier as it will impact the design and sizing of the demonstration unit, as well as the nominal power of the unit. Two minerals, ilmenite T1 and LY Mn ore, with high potential for a well performing oxygen carrier were tested in a 10kWh continuous pilot unit. The collected fines were analyzed by SEM and XRF analysis to characterize the particles' compositional and morphological evolution during operation. The performance of both oxygen carriers was compared with respect to solid fuel conversion, capacity for oxygen transfer and particle lifetime in continuous circulation. A higher methane conversion can be obtained using ilmenite, while LY Mn is better at converting petcoke. Where the reduction potential of oxygen carriers is concerned, it was observed that LY Mn ore has a high initial $R_0\Delta X$ value ($R_0\Delta X$=0.8), which leads to a shorter activation period in comparison to Ilmenite T1, which requires a longer activation period to reach its full potential. LY Mn ore is however more sensitive to attrition than ilmenite, under similar operating conditions, which is a critical characteristic for large scale deployment. Finally, key operating parameters were identified for large scale unit operation, including: FR temperature, oxygen carrier flowrate, fuel flowrate.

INTRODUCTION

In the context of the global initiative for transition from fossil fuel based to a sustainable energy system, chemical industry is investing in zero emission, alternative fuels and zero waste production models. One of the major concerns for reaching sustainability goals is the reduction of greenhouse gases in the atmosphere, among which CO_2 is the key player. It is necessary to redesign existing processes for cleaner fuels combustion, higher energy efficiency and deploy new technologies for carbon dioxide capture, use and storage (CCUS) on a large scale. Such process adjustments will require additional energy for separation of CO_2 from exhaust gas flows and for compression before injection into pipes. Thus, it is an imperative to find a technology for CO_2 separation with minimal added costs and ability to meet all the standard energy requirements (steam, hot air or electricity).

Chemical looping combustion (CLC) technology has emerged as one of the most important clean fossil fuel combustion technologies, as it allows for sequestration of CO_2 with minimal increase in energy requirements and fuel demand in comparison to traditional plants. Main characteristics of CLC process include combustion without direct contact between fuel and air and inherent sequestration of CO_2 that does not require any additional energetical input. After steam condensation, essentially pure CO_2 is obtained [1].

In a typical CLC process configuration, combustion is achieved by circulation of a metal oxide, that is termed oxygen carrier, instead of direct combustion with air, which requires a high energy consuming air separation unit. The reacting system includes two interconnected fluidized beds, the air reactor (AR) and the fuel reactor (FR). The fluidization regime in reactors can vary, and in the present work, FR and AR are operated in bubbling fluidized bed regime that should allow for extrapolation of the results for the industrial case of continuous turbulent bed coupled with a riser. In the AR, the oxygen carrier undergoes oxidation by air and an oxygen depleted air stream that is rich in nitrogen is available at the reactor outlet. The oxidized oxygen carrier is transported by entrainment to the FR, where it is reduced by the fuel (see Figure 1). The exhaust flue gas that is recovered from the FR contains only CO_2 and H_2O, where H_2O can be separated by a simple condensation operation. The fuel for combustion can be in gas, liquid or solid phase.

CLC is a technology well adapted to pulverized solid fuels, that are gasified before reacting with the oxygen carrier. At high temperatures, solid fuels release volatiles that further react with oxygen carrier particles to form CO_2 and H_2O. The solid matter that remains after the volatiles are released is termed char, which, in the presence of water vapor and/or CO_2, is susceptible to gasification and reaction with the oxygen carrier [2].

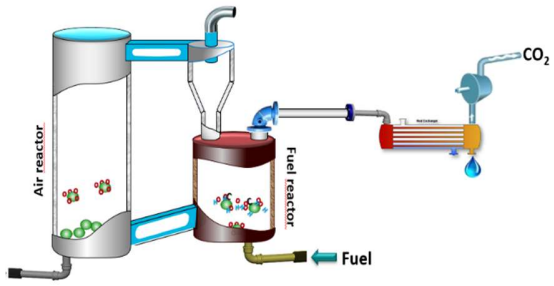

Figure 1: Diagram of chemical looping combustion process

The development of CLC technology with the goal of a large-scale deployment is of great importance, especially in the context of CO_2 capture in traditional combustion processes with pulverized solid fuels. Coal is by far the largest emitter of CO_2 from large facilities and CLC offers a significant potential for achieving zero emissions operation. [2] Significant work has been done on CLC process scale-up and technology demonstration [1–5] and it is foreseen as one of the most efficient processes for carbon capture in combustion processes. In the next stage of development, the research community turns to alternative fuels, with petcoke being particularly interesting in the context of refineries. In the scope of CLC technology scale up, it could be beneficial to increase the size of solid fuel particles so as to limit the small particle entrainment [6], while current operational experience mostly relies on solid powders application due to pilot plant size and pipeline diameters constraints.

The main requirements for oxygen carriers include high reactivity towards oxidation and reduction steps, resistance to attrition and agglomeration, and reasonable production costs [7]. The materials used as oxygen carrier will influence the size of CLC plants through their oxygen transfer capacity (OTC) and redox rates (e.g. lower redox rate material shall require a higher AR to achieve full solid oxidation). Over the years, a significant number of oxygen carriers has been tested for CLC application (synthetic materials: nickel, copper, manganese, iron, cobalt based oxides; ores or waste materials: iron, Ilmenite, manganese, calcium sulfate) [1]. Pure metal oxides rarely satisfy all the desired characteristics of an oxygen carrier. For this reason, the system of choice usually includes a combination of several metal oxides with appropriate supports. Naturally occurring minerals are particularly appealing due to their low price and high availability. Up to present, most operational experience comes from laboratory or pilot scale tests, where synthetic oxygen carriers were predominantly tested with gaseous fuels [8]. For solid fuel operation, the most common materials are naturally occurring minerals (e.g. ilmenite, iron ores, waste materials and manganese ores [8]) due to expected losses of oxygen carrier particles during ash draining from the FR [9]. In the following section, a performance overview of two most promising naturally occurring oxygen carriers: ilmenite and manganese ores is provided.

Oxygen carrier performances: Ilmenite vs. Mn ores

The selection of an appropriate oxygen carrier is one of the most important points for technology demonstration, as it represents both the fuel conversion and thermal vector of the process and is currently the most reliable parameter of process design. Possible technical risks and added costs for the equipment will be known only after commercial scale demonstration and for this reason, a focus remains on comparison of oxygen carriers. To achieve a feasible operation, the lifetime of the oxygen carrier should be sufficiently high to avoid significant costs of material supply and overturn which is why it is crucial to perform tests in circulating conditions before technology demonstration on a large scale. In the case of solid fuels, natural ores are often materials of choice, given the satisfying lifetime (several hundreds of hours) and low cost.

One of the most promising low-cost natural ores is ilmenite. Consequently, it has been widely studied in CLC continuous units at different scales (0.5 and 50 kW at ICB-CSIC [10, 11], 10 kW and 100 kW at CUT [3, 12] , 25 kW at TUHH [13], and 1 MW at TUD [14]). Each study pointed out the activation period of the material during oxydo-reduction cycles, where ilmenite's reactivity is enhanced, which can be explained by structural changes on the particle surface [13].

Similarly, there are many publications that deal with the use of manganese ores as oxygen-carrier materials in chemical-looping combustion. As compared to ilmenite, the manganese ore achieved a significantly higher rate of fuel gasification and higher gas conversion, while fines production was higher [3, 15, 16]. High reactivity of manganese ores is often related to catalytic effect of impurities (such as alkali particles) that cause cavitations in the solid char and improve char gasification rates as a consequence [17, 18]. It should be noted that the alkali effect is not sustainable over multiple redox cycles as alkali can be lost with ash. For this reason it is important to study the ore under long circulation periods at pilot scale. Schmitz et al. [5] conducted tests with three Mn-based minerals with wood char and petcoke as fuels. All three minerals achieved a higher fuel conversion compared to ilmenite, while exhibiting a significantly lower lifetime. Other explanations of high gasification rates that are observed with manganese ores come from the reactivity of OC towards H_2 (which is a known inhibitor of steam gasification) [19, 20]. However, a decrease of H_2 concentration in fluidized bed was not universally observed with all the manganese ores, so further explorations into this effect are necessary to confirm it. In reference to oxidation kinetics in AR, a theoretical design study performed by Chen et al. [21] of a 3 MWth CLC demonstration pilot unit pointed out that manganese ore had a higher oxygen transfer capacity in comparison to ilmenite. Sundqvist et al. [22–24] tested 19 different manganese ores with methane and syngas in batch operation and could show that nearly half of the manganese ores have a significantly higher reactivity with syngas as compared to ilmenite. Nearly all manganese ores tested exhibited a decrease in fuel conversion after three

redox cycles at 1000 °C [3]. However, manganese ore conversion could decrease when different fuels (syngas vs. CH_4) are tested and at lower temperatures (e.g. 850°C) [25], indicating that the reaction rate between solid fuel and ilmenite/manganese ore should be verified for the same operating consitions of fuel type, FR temperature and air/fuel ratio. Furthermore, it is well known that higher temperature of operation favours solid fuel conversion. In CLC operating conditions, the upper temperature limit for FR and AR will depend on sintering and agglomeration tendencies of the chosen oxygen carrier. In a study of melting charcateristics of Vietnamese ilmenite ore and 7 types of manganese ores [26], it was found that in both inert atmosphere (representative of AR condition) and reducing atmosphere (FR condition), manganese ores have lower melting temperatures. This is a potentially limitting factor for application of manganese ores at a large scale.

Based on the results from laboratory and pilot scale tests, it is evident that both ilmenite and manganese ore have potential to satisfy the requirements of a well-performing oxygen carrier in a CLC plant with a pulverized solid fuel. However, at present there is no operational experience at commercial or semi-commercial scale that would directly compare the performance of two natural ores and the feasibility of their operation. Since the results of small scale tests of fluidized bed technologies cannot be directly translated into large scale, there is a level of uncertanty that is inherent in CLC technology upscaling and the associated risk of investment is high [6]. For this reason, it is important to directly compare the performance of perspective OCs in a study of petcoke reactivity while taking into account the design constraints of the same industrial unit. Two naturally occuring ores, ilmenite and manganese ore, were characterized and compared in the scope of the CHEERS project and the main conclusions of performance testing in a circulating unit of 10 kWth capacity are provided in this work..

Scope of the work

The CHEERS project is part of the European Horizon 2020 Work Program 2016 – 2017, 10. 'Secure, Clean and Efficient Energy', under the low-carbon energy initiative (LCE-29-2017: CCS in Industry, including BioCCS). Within the framework of CHEERS, the core technology of CLC process is to be developed into a 3 MWth system prototype for demonstration in an operational environment. This constitutes a major step towards large-scale decarbonization of industry, offering a considerable potential for retrofitting industrial combustion processes.

The system prototype is based on a fundamentally new fuel-conversion process designed from prior research and development actions over more than a decade. The system will include heat recovery, steam generation, flue gas treatment, and it will comply with industrial standards, specifications and safety regulations. Except for CO_2 compression work, the innovative concept is capable of removing 96% of the CO_2 while eliminating capture losses to almost zero.

One of the main objectives of the CHEERS project is the selection of the most promising oxygen carrier as it will impact the design and sizing of the demonstration unit, as well as the nominal power of the unit. It is important to say that the demonstration unit will be operated in a turbulent fluidized bed regime, where an increase in mass transfer coefficient is expected with respect to the bubbling bed fluidized regime at pilot scale (up to 1 MW_{th} power) that sees large fractions of gas by-passing and poor mass transfer [8].

To select the best candidate, the OC is first tested in a batch reactor by fuel feeding of methane or petcoke. In addition, to evaluate fuel conversion and oxygen transfer capacity, a special attention is given to the formation of fines (due to attrition) and agglomerates. Second, tests are conducted in a continuous pilot unit (described in section Experimental method) to ascertain the material's performances (fuel conversion, oxygen transfer capacity) when relevant hydrodynamic behavior (bubbling fluidized bed, particle entrainment, L-valve mechanical transfer and cyclonic separation) is considered. Furthermore, these tests allow for a closer estimation of oxygen carrier lifetime, by evaluating the amount of fines formation as a function of time, as well as morphology changes due to solid circulation. Each of the test campaigns is followed by structural characterization of the oxygen carrier to highlight phase changes in relation to reactivity evolution, particle strength and affinity for agglomeration. However, both units were operated in a hydrodynamic regime (bubbling regime) not representative of the demonstration unit hydrodynamic regime.

To extrapolate the performance to the demonstration unit, a model has been developed based on kinetic laws determined in the batch unit cited above. Then, the kinetic laws have been validated by experimental results obtained in the continuous pilot. Finally, a turbulent hydrodynamic regime has been implemented in the model, allowing to simulate the CHEERS demonstration unit (The aforementioned model will not be discussed in this work). The experimental data from demonstration unit operation will be used to validate the final model.

In the demonstration unit, higher solid fuel conversion is expected since the residence time will be more important than in the pilot unit. Attrition behavior in the demonstration unit is expected to be similar to the one observed in the continuous unit (or even lower since gas velocity in FR nozzles for fluidization is important in the pilot unit). Agglomeration issues are expected to occur but with less impact as the pipeline diameters will be larger. To achieve a higher conversion of volatiles with solid fuel operation, different operating strategies could be employed such as: using ring-type internals, using a secondary fuel reactor or employing carbon stripper as the primary fuel reactor by feeding the solid fuel to carbon stripper first [9]. If the existing CLC configuration is kept, gas/solid contacting could be improved by using turbulent fluidized bed regime instead of bubbling fluidized bed.

The scope of this paper includes:

I. Summary of the experiences from continuous pilot operation with respect to important performance parameters with an ilmenite and a manganese ore as oxygen carriers

II. Comparison of both oxygen carriers with respect to industrial scale application in demonstration unit.

Materials

The oxygen carriers (OCs) used in this study are an iron-manganese ore called "LY Mn ore" mined in China and an ilmenite from Titania AS mined in Norway. Their structural characteristics are discussed in section Structural and morphological evolution of the oxygen carriers.

The particle size distribution of as-received oxygen carriers, determined by laser diffraction analysis, is given in Figure 2. It appears that about 30 % of the total mass of the LY Mn ore is below 100 µm, so the material was sieved in the 100-300 µm range to allow a good circulation of particles in the continuous pilot unit. Ilmenite has been received in the 100-300 µm range.

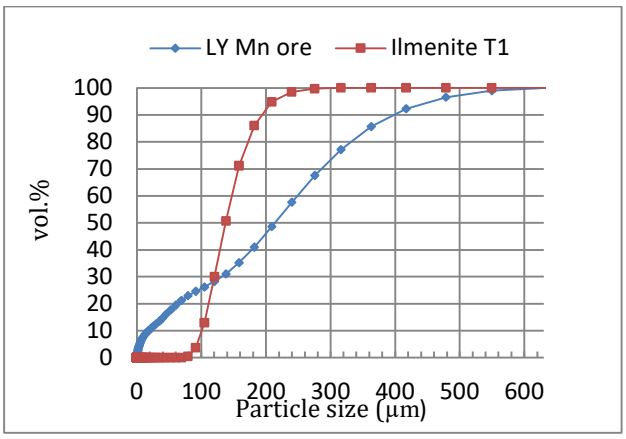

Figure 2: Particle Size Distribution of OCs (red: ilmenite, blue: LY Mn ore)

Experimental method

Note that the experimental results obtained in the batch unit will not be discussed in this paper.

A schematic view of IFPEN's 10 kW CLC continuous pilot unit used in this campaign is shown in Figure 3.

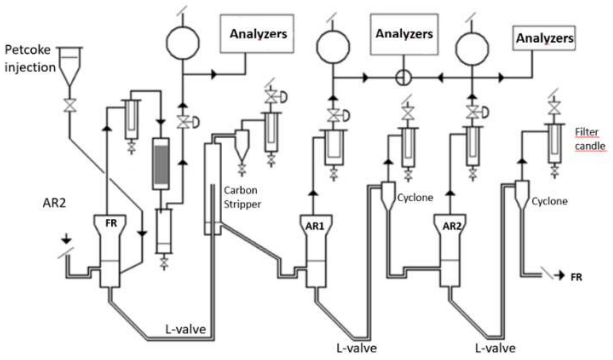

Figure 3: schematic view of IFPEN's 10 kW_{th} unit

The pilot is composed of three interconnected bubbling fluidized bed reactors and a carbon stripper. Two fluidized bed reactors (AR1 and AR2) are dedicated to the oxygen carrier oxidation and the third one (FR) is dedicated to fuel combustion, therefore performing OC reduction. In the fuel reactor, gaseous fuel or petcoke can be injected to react with the oxygen carrier and reduce it. The reduced particles go through the carbon stripper (CS) before entering the air reactor AR1. This CS has been implemented to separate unburnt carbon compounds from the OC in the case of solid fuels combustion (herein, petcoke combustion).

The solid circulation systems are identical from AR1 to AR2 and from AR2 to FR. The oxygen carrier leaving the reactors (AR1 or AR2) by the bottom enters a pneumatic L-valve of 0.017 m i.d. and 1.1 m length. From that point, the solid is transported through a lift with 0.02 m i.d. and 2.25 m height and then enters a horizontal dilute phase conveying line. Finally, the conveying gas and solid are separated in a cyclone. Then, the OC particles go through a loop seal upstream to the next reactor (AR2 or FR). This loop seal, fluidized with nitrogen, allows avoiding any gas transfer between the reactor gas phase and the conveying gas transporting the solid to the cyclone. Between the FR and AR1, the solid leaving the reactor by the bottom goes through a pneumatic L-valve and is transported to the carbon stripper through a lift. The carbon stripper separates the particles according to their volume and density, the lightest particles get entrained by the gas, while the heaviest fall down, leave the carbon stripper by the bottom and enter a loop seal connected to the air reactor AR1. The fuel reactor (FR) has an internal diameter of 0.13 m and is fluidized with nitrogen and methane in gas combustion mode, or nitrogen and water vapor in solid combustion mode. The total flow rate of the fluidizing gas is chosen to operate at 3 times the minimum fluidization velocity of the OC to ensure a sufficient fluidization. By configuration, both air reactors (AR1 and AR2) can be fed with air (in operation) or nitrogen (inert in emergency shutdown procedures). As in the fuel reactor, the total flow rates used are chosen to obtain a good fluidization of the particles.The CLC pilot unit is equipped with three multi-gas online analyzers. CH_4, CO and CO_2 concentrations are continuously measured at the outlet of the FR by non-

dispersive (NDIR) infrared analyzers (ABB-URAS 26), while H_2 concentration is analyzed by a thermal conductivity detector (ABB-Aldos 27). In AR1, CO, CO_2 and O_2 concentrations are determined by a combined NDIR-paramagnetic analyzer (ABB-Uras 26 /Magnos 206). Finally, in AR2, O_2 is measured by an electrochemical cell analyzer (Siemens – Ultramat 23).Several measurements were performed on the OCs (Table 1) prior to reactor loading.

Table 1: pre-measurements of oxygen carrier properties

	Ly Mn ore	**Ilmenite**
Bulk density (g/cm^3)	*2,11*	*2,31*
Humidity (wt%)	*0.24*	*< 0.01*
Mean particle diameter (µm)	*200*	*203*
Minimum fluidization velocity (cm/s)	*8*	*7.4*

The value of the total inlet gas flow rate in the reactors has been chosen to operate between 2 and 3 times of the minimal fluidization velocity of the OCs to ensure proper fluidization regime. Minimal fluidization velocity has been determined experimentally in a small fluidized bed reactor at room temperature.

Fuel characteristics

Fuels used in this study were:

a. Methane, mainly to activate the OC, from Air products (purity of 99.95 %v)
b. Petcoke, named Petcoke C5LS (Chinese 5 low sulfur solid).

The elemental analysis of this petcoke was obtained by performing thermal conductivity analysis (for C,H and N contents) and IR spectroscopy (for O and S contents) and the results are reported in Table 2. The particle size distribution of this petcoke ranged between 100 and 315 µm.

Table 2: Elemental analysis of petcoke C5LS

Elemental analysis (wt%)				
C (%)	H (%)	O (%)	N (%)	S (%)
90.8	4.02	1.58	1.84	0.35

Proximate analysis of the petcoke C5LS is given in Table 3, determined by TGA mesurement.

Table 3: Proximate analysis of petcoke C5LS

Proximate analysis (wt%)			
Fixed-C	Volatiles	Water	Ash
87,5	11.4	0.57	0.5

Evaluation of reactivity and performance of the OC

Three parameters are investigated to evaluate the reactivity and performance of the OC:

a. The quantity of oxygen released in the fuel reactor $R_0\Delta X$ (wt%)
b. The fuel conversion (methane or petcoke)
c. The CO/CO_2 ratio, which is linked to the oxygen carrier efficiency

The quantity of oxygen released by the material is represented by the $R_0\Delta X$ value, where ΔX corresponds to the conversion of the oxygen carrier in the fuel reactor and R_0 corresponds to the oxygen transfer capacity of the fresh material. The mathematical expression can be found in

Table 4 (see Equation 1) that provides an overview of all the equations that were used for quantification of oxygen carrier reactivity and performance. The $R_0\Delta X$ parameter can be calculated in two different ways (Equations 2 and 3) if the oxygen mass balance is performed on the fuel or the air reactor.

The petcoke flowrate leaving the fuel reactor ($Q^{FR}_{petC,out}$) is divided in two flows. The petcoke dragged away with the gases ($Q^{FR}_{petC,out,g}$) and the petcoke leaving with the oxygen carrier by the reactor's bottom ($Q^{FR}_{petC,out,OC}$).

Using the samples collected at the fuel reactor outlet, which contain petcoke and oxygen carrier, it is possible to calculate the unburnt petcoke flowrate leaving the reactor with the gases ($Q^{FR}_{petC,out,g}$). Indeed, these samples are calcined in an oven and, correcting for ilmenite weight gain during reoxidation using the $R_0\Delta X$ value, the variation of mass before ($m^{FR}_{red+P,out}$) and after the combustion ($m^{FR}_{ox,out}$) is linked to the petcoke content. The amount of petcoke dragged away with the gas flowrate is calculated as presented in equation 4 and 5 (with $m^{FR}_{petC,out,g}$ the mass of petcoke retrieve at the fuel reactor filter (kg)).

In equation 6, it is assumed that petcoke CHONS composition is not impacted by its conversion. To confirm this hypothesis, petcoke samples were collected at different conversion levels in a batch test unit and standard CHONS analysis was performed. Data showed very limited changes (see Table 5.) in petcoke CHONS composition and the model assumption holds.

A similar equation is used to calculate the petcoke flowrate entering air reactor 1 (equation 7) (with $m^{CCS}_{petC,out}$ the mass of petcoke retrieved at the carbon stripper cyclone (kg)).

Methane conversion (X_{CH4}) in the fuel reactor can be calculated from Equation 8. It is largely impacted by the solid and gas residence time in the reactor. With $F^{FR}_{gas,in}$ the FR inlet total molar flow rate of the gas phase (mol/s), $x^{FR}_{CH_4,in}$ the fraction of methane at the inlet of the FR (-), $F^{FR}_{gas,out}$ the FR outlet total molar flow rate of the gas phase (mol/s), $x^{FR}_{j,out}$ the fraction of component j at the outlet of the FR (-) with j being CO_2, CO or CH_4. Petcoke conversion ($X_{petcoke}$) can be calculated from Equation 9.

The ratio between CO and CO_2 (CO/CO_2), representing a quality of combustion, is calculated from Equation 10. If the combustion is total, this ratio equals to zero, but if the oxygen carrier is not able to oxidize all the carbon monoxide or hydrogen produced by the fuel conversion, this ratio increases and a mixture of CO, H_2, CO_2 and H_2O is obtained at the fuel reactor outlet. At similar fuel conversion, the operating conditions leading to a lower CO/CO_2 ratio must be favored. Carbon capture efficiency (ηCC) over the reaction section is calculated from equation 11.

Table 4: Equation chart for evaluation of reactivity and performance of OC

Eq N°	*Equation*
1.	$$\boldsymbol{R_0 = \frac{m_{Oavailable}}{m_{solid}}}$$
2.	$$\boldsymbol{R_0 \Delta X_{FR} = \frac{\left(\int_{t_0}^{t_f}\left(2F_{CO_2,out}^{FR} + F_{CO,out}^{FR} - F_{H_2O,in}^{FR} - F_{petC,in}^{FR}\right)dt + \frac{m_{H_2O}^{condenser}}{M_{H_2O}}\right)M_O}{\int_{t_0}^{t_f} Q_{m,s}\, dt}}$$
3.	$$\boldsymbol{R_0 \Delta X_{AR} = \frac{\left(\int_{t_0}^{t_f}\left(2F_{O_2,in}^{AR1} + 2F_{O_2,in}^{AR2} - 2F_{CO_2,out}^{AR1} - F_{CO,out}^{AR1} - 2F_{O_2,out}^{AR1} - 2F_{O_2,out}^{AR2}\right)dt\right)M_O}{\int_{t_0}^{t_f} Q_{m,s}\, dt}}$$
4.	$$\boldsymbol{m_{petC,out,g}^{FR} = m_{red+P,out}^{FR} - m_{ox,out}^{FR}(1 - R_0 \Delta X)}$$
5.	$$\boldsymbol{Q_{petC,out,g}^{FR} = \frac{m_{petC,out}^{FR}}{(t_f - t_0)}}$$
6.	$$\boldsymbol{Q_{petC,out,OC}^{FR} = \frac{\left(\int_{t_0}^{t_f} Q_{petC,in}^{FR}\, dt - m_{petC,out}^{FR}\right)C_{petC,in} - \left(\int_{t_0}^{t_f}\left(F_{CO_2,out}^{FR} + F_{CO,out}^{FR}\right)dt\right)M_C}{(t_f - t_0)C_{petC,in}}}$$
7.	$$\boldsymbol{Q_{petC,in}^{AR1} = \frac{\left(\int_{t_0}^{t_f} Q_{petC,in}^{FR}\, dt - m_{petC,out}^{FR} - m_{petC,out}^{CCS}\right)C_{petC,in} - \left(\int_{t_0}^{t_f}\left(F_{CO_2,out}^{FR} + F_{CO,out}^{FR}\right)dt\right)M_C}{(t_f - t_0)C_{petC,in}}}$$
8.	$$\boldsymbol{X_{CH4} = \frac{\left(F_{gas,in}^{FR} * x_{CH_4,in}^{FR} - F_{gas,out}^{FR} * x_{CH_4,out}^{FR}\right)}{F_{gas,in}^{FR} * x_{CH_4,in}^{FR}}}$$
9.	$$\boldsymbol{X_{petcoke} = \frac{\left(\int_{t_0}^{t_f}\left(F_{CO_2,out}^{FR} + F_{CO,out}^{FR}\right)dt\right)M_C}{Q_{petC,in}^{FR}(t_f - t_0)C_{petC,in}}}$$
10.	$$\boldsymbol{\frac{CO}{CO2} = \frac{F_{gas,out}^{FR} * x_{CO,out}^{FR}}{F_{gas,out}^{FR} * x_{CO_2,out}^{FR}} = \frac{x_{CO,out}^{FR}}{x_{CO_2,out}^{FR}}}$$
11.	$$\boldsymbol{\eta CC = \frac{F_{CO2,FR}^{out} + F_{CO,FR}^{out} + F_{CH4,FR}^{out} - F_{CO2,FR}^{in}}{F_{CO2,FR}^{out} + F_{CO,FR}^{out} + F_{CH4,FR}^{out} + F_{CO2,AR1}^{out} + F_{CO2,AR2}^{out} - F_{CO2,FR}^{in}}}$$

* with $t_f - t_0$ standing for the duration of the mass balance (s), F_j^i the molar flow rate of component j at the inlet/outlet of reactor i (mol.s^{-1}), $m_{H_2O}^{condenser}$ the mass of water obtained at the condenser of the fuel reactor during the duration of the mass balance (kg), $Q_{petC,in\ or\ out}^{unit}$ the mass flowrate of petcoke at unit inlet or outlet (kg s^{-1}), $O_{petC,in}$ the oxygen content of the inlet petcoke (kg/kg) and $Q_{m,s}$ the solid flow rate (kg s^{-1}).

Table 5: Evolution of petcoke CHONS composition for various petcoke conversions

$X_{petcoke}$ (%)	C (%)	H (%)	O (%)	N (%)	S (%)
0	96.5±0.7	0.92±0.1	0.31±0.1	1.36±0.1	0.74±0.1
20	96.6±0.7	0.65±0.1	0.49±0.1	1.31±0.1	0.93±0.1
50	96.1±0.7	0.51±0.1	0.43±0.1	1.26±0.1	1.03±0.1

Operating conditions

The performance of the CLC process depends on the selected operating conditions, among which:

- Reactors' temperature:

The temperature of the reactors is controlled on the pilot unit with heating wire. The fuel reactor (FR) temperature can be modified for each test. It was varied between 900 and 950 °C with a value of 900 °C for most of the tests. Since petcoke requires a high temperature to reach good conversion, lower temperatures were not studied.

The target temperature of both air reactors was set at 850 °C for each test.

- Reactors gas flow rates:

The reactors inlet gas flow is composed of steam and nitrogen (and methane in gas combustion mode) for the FR and air for the air reactors (AR1 and AR2).

The value of the total inlet gas flow rate in the FR has been chosen to operate between 2 and 3 times the minimal fluidization velocity of the OC to ensure proper fluidization regime.

The inlet gas flow rates of the air reactors are adjusted to obtain a high oxidation level of the material in both reactors to ensure a fully oxidized state of the material at the inlet of the fuel reactor. The total gas flow rate used in these reactors is generally around 2 Nm^3/h which corresponds to a superficial velocity around 5 times the minimal fluidization velocity.

In the tests at varying temperatures, the total gas flow rate has been adjusted to maintain the required gas velocity in the fuel reactor.

- Methane concentration:

During OC activation, the operating conditions have been adjusted progressively to reach a constant $R_0\Delta X$ value. The methane concentration at fuel reactor inlet was varied from 2 to 10 %v which corresponds to a variation of power from 0.4 to 2 kW.

- Solid flow rate:

The solid flow rate can be controlled in the unit thanks to the use of L-valves. When leaving a reactor, the OC proceeds through an L-valve which is used to regulate the solid flow rate injected in the subsequent riser. To determine solid flowrates, a specific riser pressure drop is imposed and the bed levels of the air and fuel reactor are recorded. From this data, it is possible to calculate a solid flowrate depending on the pressure drop in the riser. With this device, the solid flow rate is controlled by the gas flow rate injected in the L-valve. The pressure drop in the lift is directly linked to the solid flow rate and a correlation between the solid flow rate and the lift pressure drop has been established for ilmenite and LY Mn ore before the study (Figure 4). The empirical model for solid flowrate calibration curve was calculated from hot flow tests ($T_{FR} = 720°C, T_{AR} = 740°C$) where AR2 was filled with solids and as the solids were transferred from AR2 to FR, the pressure drop in the lift was continuously measured. For the average value of pressure drop in both reactors during the test, the associated mass flowrate of solids was calculated from the lift geometry (Equation 12):

Equation 12 $$\dot{m} = \frac{A_{pipe}}{g} * \frac{\Delta p}{\Delta t}$$

Where A_{pipe} is internal area of the lift pipe (m^2), g is gravitational acceleration (m/s^2) and $\frac{\Delta p}{\Delta t}$ is the average value of pressure drop in AR2 and FR (kg/ms^3). Measurements were repeated at several experimental points to obtain the calibration curve.

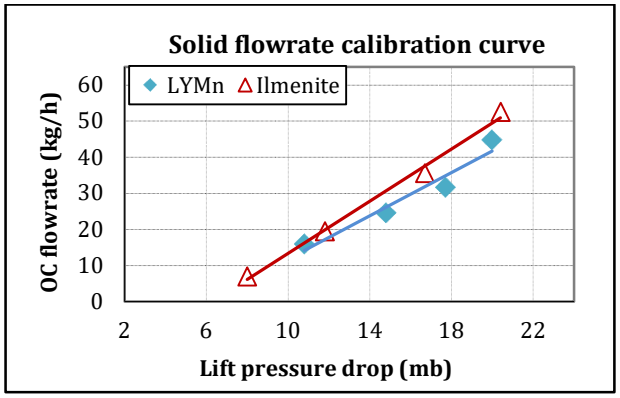

Figure 4 : Calibration curve of the solid flow rate in the unit over the pressure drop in the lift after AR2

- Solid inventory in each reactor:

The impact on process performance of the solid inventory in the fuel reactor has been studied. The solid flowrates between reactors are adjusted with L-valves, which allows having a total control of the solid levels in the unit. Unless specified, the tests have been performed at constant levels of solid in the fuel

reactor. The solid levels of the air reactors are adjusted to remain equal to each other whatever the total solid inventory.

Results and discussion

For each study, the experimental procedure was as follows:

a. Ageing of the OC and characterization of its reactivity and morphology variations over time under gaseous fuel (CH_4).
b. influence of the following parameters during solid fuel (petcoke) gasification:
    - the fuel reactor (FR) temperature,
    - the oxygen carrier flow rate,
    - the petcoke flow rate,
    - the solid level in the FR,
    - the steam concentration

Key performance indicators

To calculate the three parameters for evaluating the reactivity and performance of each OC (fuel conversion, $R_0\Delta X$ and CO/CO_2 ratio…), mass balances are performed during a certain period of time when the system is stabilized. During this period, the fuel is continuously converted into CO, CO_2, H_2O and H_2 at the outlet of FR. The measuring devices of CO, CO_2 and H_2 concentrations have already been described in Experimental method section. Water is collected in a condenser at the outlet of the FR.

Methane activation

In this paper, both materials were activated under methane to reach steady state condition. In the start-up procedure for the demonstration unit, this will be achieved by direct exposure to petcoke. Materials were activated under methane to provide results on equilibrium state performance of the material that will be more representative of normal operation. It should be noted that the available loadings of both OCs were different for the two campaigns (lower mass of LY Mn available for the circulation, in comparison to ilmenite), That is why the achieved bed levels in the fuel reactor (HFR) for both campaigns were different.

The main operating conditions during ilmenite activation are presented in

Table 6. After an average of 60 reduction/oxidation cycles (corresponding to ~70h methane combustion), ilmenite reactivity was stabilized (more than three days of operation). After 30 more hours of combustion (and 30 additional reduction/oxidation cycles), the unit had to be stopped due to agglomeration troubles in the fuel reactor L-valve and instabilities at the fuel reactor outlet cyclone. The cyclone instabilities were solved easily by a pressure adjustment, but the plugging of the L-valve required to cool the unit down and clean it manually. By the end of the ilmenite stabilization period, $R_0\Delta X$ and methane conversion reached respectively a value of 1.25 and 68.0% for a methane inlet in the fluidization gas of 7.5%v (

Table 6, mass balance 8).

The carbon capture efficiency, calculated using Equation 11, is close to 99 % for all the tests under methane.

The main operating conditions used during the activation with methane as fuel and with LY Mn ore as OC are given in Table 7, as well as the methane conversion and mean $R_0\Delta X$ for each mass balance. The tests have been performed at constant levels of solid in the fuel reactor (except for mass balance 10, where the effect of increasing the bed height was tested).

By the end of the stabilization period, $R_0\Delta X$ and methane conversion reach respectively a value of 1 and 35.5 % (Table 7, mass balance 12 and 13). Mass balance n°10 is not representative of the activation of the OC since the FR bed level was higher than the bed levels in the other mass balances. However, this shows that the FR bed level (and in this case the gas residence time in the FR) impacts the methane conversion and $R_0\Delta X$.

Experimental results of LY Mn ore activation, with respect to methane conversion evolution and value of $R_0\Delta X$ are provided in graphical representations in Figure 5, in comparison to Ilmenite T1.

Table 6 : Operating conditions during all the mass balances performed during the activation with methane and performance of ilmenite as OC (conversion, $R_0\Delta X$ and CO/CO_2 ratio)

Balance	FR T (°C)	AR1 T (°C)	AR2 T (°C)	HFR (cm)	OC flowrate (kg/h)	CH4 in (v%)	R0ΔX (%)	X_{CH4} (%)	CO/CO2
1	898	739	712	54	20.6	2.0	0.39	56.9	0
2	900	756	760	55	20.6	2.4	0.41	63.7	0
3	902	748	755	49	20.6	2.4	0.47	62.4	0
4	897	756	761	49	20.6	3.8	0.65	59.7	0
5	900	752	757	50	20.6	4.8	0.79	60	0.001
6	901	764	759	51	20.7	7.5	1.28	65.8	0.005
7	900	758	760	52	20.7	7.5	1.31	67.8	0.004

8	903	782	756	53	20.4	7.5	1.25	68.0	0.002

Table 7: Operating conditions during all the mass balances performed during the activation with methane and performance with LY-Mn ore as OC

Balance	FR T (°C)	AR1 T (°C)	AR2 T (°C)	HFR (cm)	OC flowrate (kg/h)	CH4 in (%v)	R0ΔX (%)	X_{CH4} (%)	CO/CO2 (/)
1	892	731	759	43	19.3	5	0.48	39.8	0.028
2	895	804	759	41	20.1	10	0.8	31.4	0.033
3	893	799	769	41	21.2	10	0.66	26.6	0.038
4	899	750	770	41	23.2	5	0.41	34.1	0.038
5	901	755	773	41	22.2	5	0.45	32.5	0.036
6	899	739	770	43	19.1	2.5	0.29	39.5	0.036
7	902	798	818	42	20.7	2.5	0.35	49.7	0.12
8	903	852	834	40	21.8	2.5	0.18	29.2	0.012
9	900	823	830	41	20.3	10	0.9	37.3	0.027
10	901	807	818	53	20.3	10	1.0	39.3	0.023
11	899	851	835	41	20.2	10	0.85	35	0.028
12	901	776	780	41	18.7	10	0.99	35.6	0.022
13	900	799	782	42	18.6	10	0.99	35.5	0.022

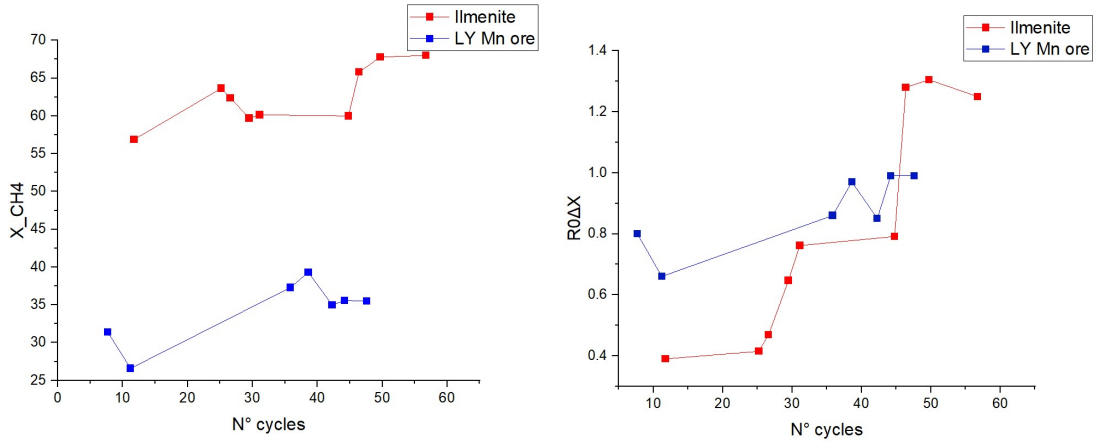

Figure 5: Evolution of methane conversion and R_0DX during LY Mn ore activation cycles in comparison to Ilmenite T1 behavior

It can be observed from Figure 5 that LY Mn ore achieves lower conversion of methane in comparison to ilmenite T1. Regarding the oxygen carrier conversion, the activation period for LY Mn ore is shorter. The limited increase in methane conversion values of LY Mn ore is consistent with changes in $R_0\Delta X$, since both trends indicate an overall lower degree of changes in the material, with respect to Ilmenite T1, which required significant activation of its redox potential. The reactivity of ilmenite is known to increase during the first period of operation. Larring et al. [27] found that costly activation of manganese ores prior to utilization in a CLC process is not always necessary since it does not improve significantly the early performance of the ore, contrary to Ilmenite.

Petcoke reactivity tests

The second part of the study focused on the influence of several parameters on petcoke gasification. The operating conditions with ilmenite and LY Mn ore are described in Table 8 and

Table 10, respectively.

For each operating condition, the gas phase leaving the reactors was analyzed and oxygen carrier samples were taken at FR, CS and AR1 outlets. Mass balances were performed to characterize the combustion efficiency of the process. The carbon, oxygen and hydrogen mass balances were evaluated by integrating the concentration profiles of CO, CO_2, H_2 and CH_4 at the outlet of the fuel reactor and the concentration of CO_2

and CO at the outlet of the air reactors. The water produced in the fuel reactor was collected in a condenser and weighed. Table 8 and

Table 10

Table 10 present the petcoke conversion and $R_0\Delta X$ for the reference case and with variations of several parameters. In the reference case, ilmenite achieves higher $R_0\Delta X$ than LY Mn ore (1.05% with respect to 0.74% with LY Mn) which could be partly explained by higher OC loading (HFR) at the fuel reactor (HFR=53 cm where HFR=43 cm in LY Mn ore reference case). The conversion of petcoke is higher with LY Mn as OC, as shown in Table 8 and

Table 10. Furthermore, Carbon Captur Efficiency (ηCC) is lower with ilmenite as OC during petcoke operation (varying from 71.1 to 80.6 on average) than with LY Mn ore (varying from 75.9 to 90.8 on average). This confirms a better activity of the Manganese ore towards solid fuel conversion.

Table **9** and Table 11 show average concentration values at FR outlet for respectively ilmenite and LY Mn ore in different operating conditions. For both OCs, the strongest effect on CO_2 content at the outlet of the FR is achieved by variation of the steam content.

Table 8: Performance of ilmenite during petcoke operation

Test type	Steam content	Petcoke flowrate	FR T	OC flowrate	HFR	$R_0\Delta X$	$X_{petcoke}$	CO/CO_2	ηCC
Units	%	g/h	°C	kg/h	cm	%	%	/	%
Reference value	49	118	927	20	53	1.05	65	0.031	76.5
FR temperature	50	110	904	21	55	0.91	59	0.034	72.3
Petcoke flowrate	50	258	928	21	51	1.83	51	0.050	79.4
FR bed level	50	114	929	22	66	0.90	64	0.028	81.3
Steam content	31	115	929	21	52	0.49	53	0.030	71.1
OC flow rate	50	119	922	10	51	2.31	73	0.051	80.6

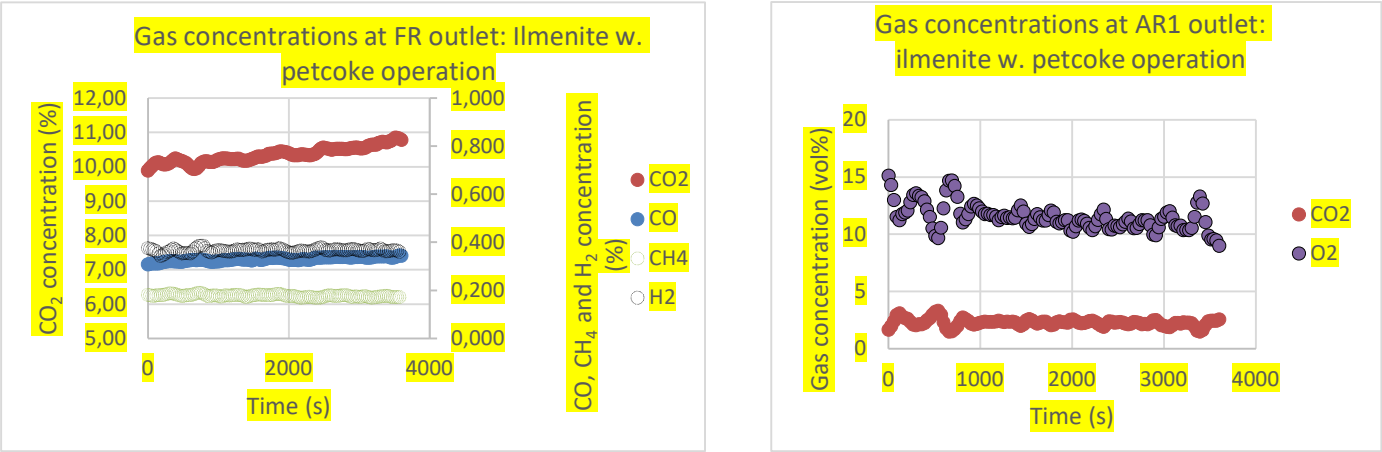

Figure 6 : Profiles of gas concentrations at outlet of FR and AR1 during a reference test with solid fuel and Ilmenite as OC

Table 9: Average gas concentration values at FR outlet for petcoke operation and parameter sensitivity tests with ilmenite

Test type	CO_2 content	CO content	CH_4 content	H_2 content
Units	%	%	%	%
Reference test	10.3	0.33	0.18	0.37
FR temperature	10.4	0.36	0.23	0.39
Petcoke flowrate	20,7	0.36	0.23	0 .39

FR bed level	10.9	0.31	0.14	0.26
Steam content	6.9	0.21	0.10	0.27
OC flow rate	11.7	0.60	0.25	0.58

Table 10 : Performance of the LY-Mn ore during petcoke operation

Test type	**Steam content**	**Petcoke flowrate**	**FR T**	**OC flowrate**	**HFR**	**R0ΔX**	**Petcoke conversion**	**CO/CO_2**	**ηCC**
Unit	*%*	*g/h*	*°C*	*kg/h*	*cm*	*%*	*%*	*/*	
Reference	50	121	934	20.0	43.0	0.74	83.4	0.045	84.2
FR temperature	50	121	904	20.1	42.38	0.55	75	0.053	75.9
Petcoke flowrate	50	244	930	20.1	43.3	1.69	81.9	0.045	83.2
Steam content	30	121	932	19.9	43.4	0.79	78.8	0.040	80.4
OC flow rate	50	121	920	29.9	45.6	0.48	88.9	0.014	90.8

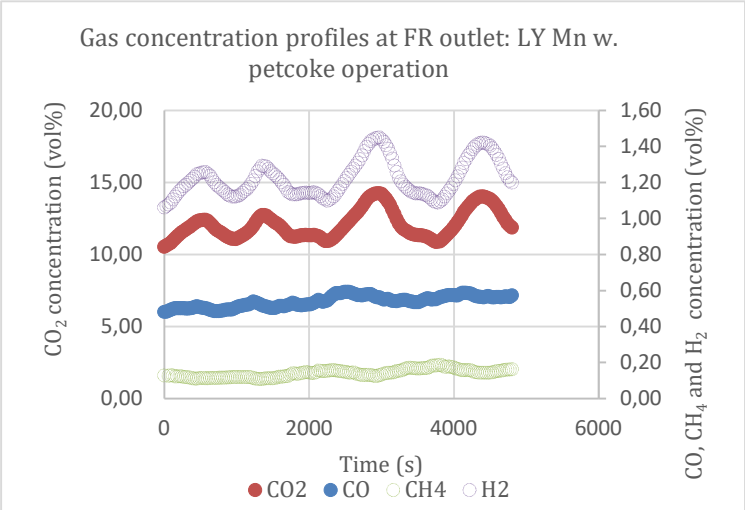

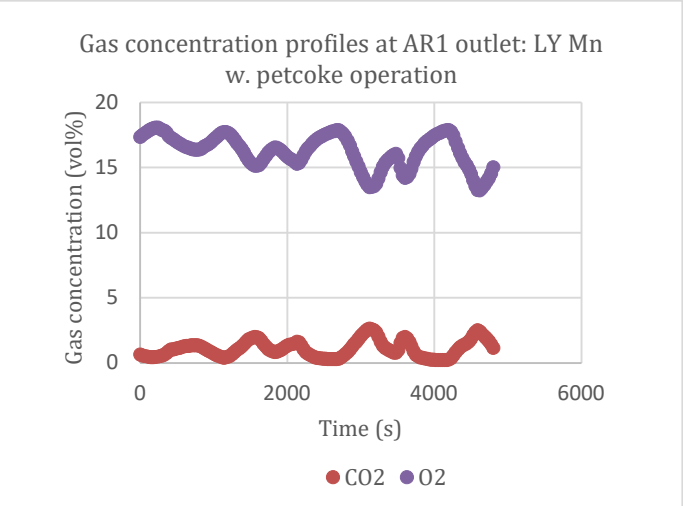

Figure 7: Profiles of gas concentrations at outlet of FR and AR1 during a reference test with solid fuel an LY Mn ore

Table 11: Average gas concentration values at FR outlet during petcoke operation and parameter sensitivity tests with LY Mn ore

Test type	**CO_2 content**	**CO content**	**CH_4 content**	**H_2 content**
Units	%	%	%	%
Reference value	12.1	0.54	0.14	1.2
FR temperature	11.3	0.61	0.16	1.14
Petcoke flowrate	19.8	0.90	0.45	1.99
Steam content	7.9	0.33	0.11	0.80
OC flow rate	11.4	0.16	0.05	1.15

Table 12 Gas concentrations (vol%) at AR1 outlet for reference cases with solid fuel

Oxygen carrier	***CO_2 (%v)***	***CO (%v)***

LY Mn	1.08	≈0
Ilmenite	2.30	≈0

Gas concentration profiles at outlet of FR show an increase in CO_2 concentration from 10 to 11 vol% for Ilmenite (Figure 6) and from 10 to 14 vol% for LY Mn ore (Figure 7) during operation, and low values of CO concentration throughout the test: 0.33 vol% for Ilmenite and 0.54 for LY Mn, indicating a better fuel gasification condition with LY Mn ore and incomplete combustion condition in both cases. The trend of higher average concentration of H_2 vol% for ilmenite (Figure 6) indicates that it had higher affinity for H_2 oxidation in the achieved test conditions, which in turn helps steam gasification of char, since H_2 is an inhibitor of this reaction [20]. However, to further study this effect and reach a conclusion on reaction with H_2, a dedicated test would be necessary, with identical OC loading in the system. Methane measured at the FR outlet is very limited and low in value for both oxygen carriers, which suggests good volatiles conversion in the reactor. It is possible to relate the registered volatiles at FR outlet to bubbling fluidized bed condition in the reactor, as poor contact between reacting gases and solid OC particles [9] is the main contributor to unconverted gases concentration. At the outlet of the first AR, low concentration of CO_2 is registered (approx. 2vol% for both OC) which is the measure of non-captured CO_2 that is lost in direct combustion with air in AR. Interestingly, in the case of LY Mn ore, significantly higher O_2 levels are registered at AR1 outlet (16 vol% in comparison to 12vol% observed with Ilmenite) which shows that the uptake of oxygen is better in the case of Ilmenite than LY Mn ore.

Leaking of char from the FR to AR1 can be followed by the CO and CO_2 concentration at the outlet of AR1 (Table 12). Average values from reference test cases with solid fuel show that incomplete combustion is achieved in the FR, with lower amounts of unconverted char in the case of LY Mn ore.

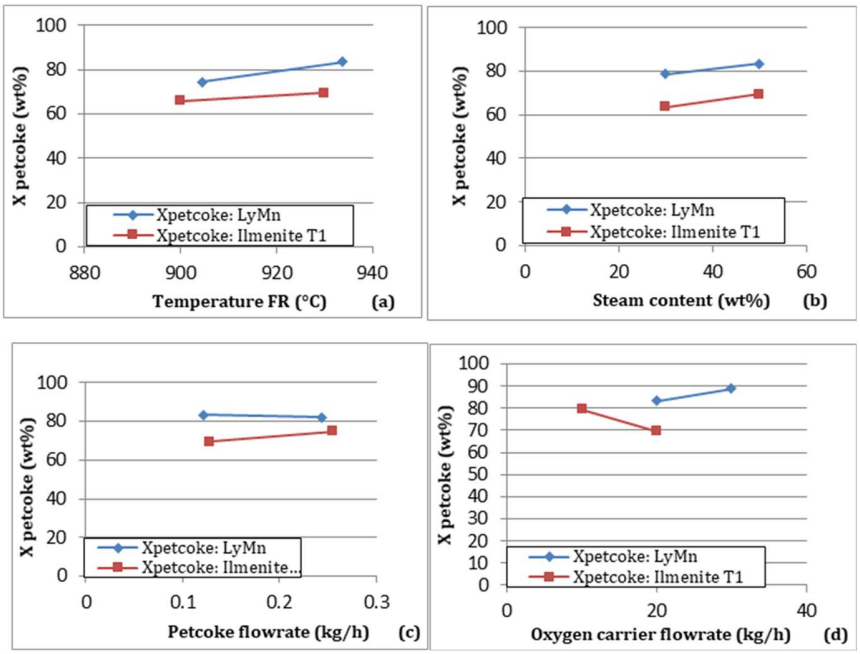

Figure 8: Evolution of petcoke conversion with: (a) temperature of FR, (b) steam content, (c) petcoke flowrate, (d) oxygen carrier flowrate for Ilmenite T1 and LY Mn ore

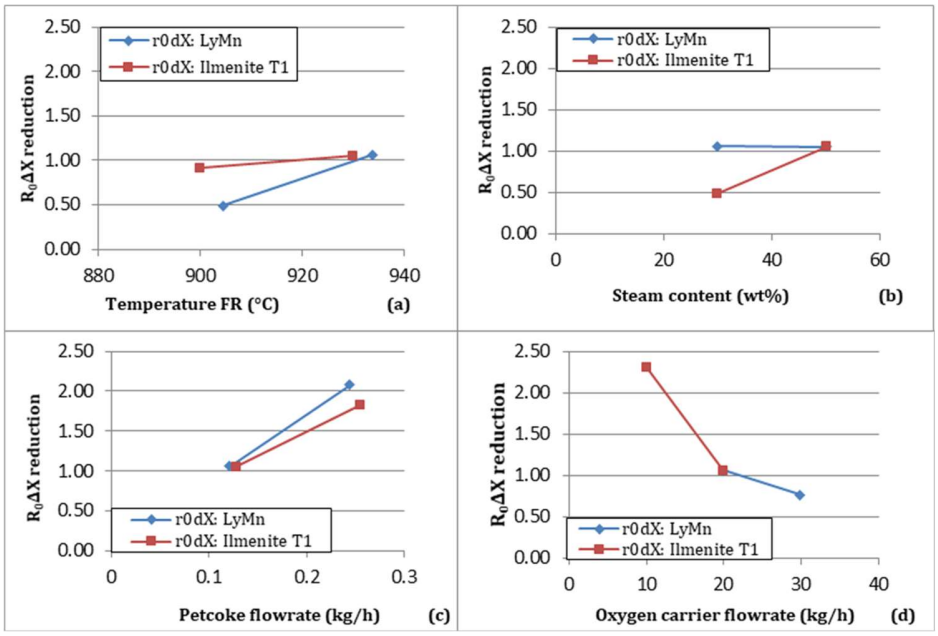

Figure 9: Evolution of $R_0\Delta X$ with: (a) temperature of FR, (b) steam content, (c) petcoke flowrate, (d) oxygen carrier flowrate for Ilmenite T1 and LY Mn ore

The following observations could be made with respect to changes in critical manipulable variables and their effects on principal reactivity indicators (R0ΔX and $X_{petcoke}$):

Temperature: Temperature increase has a positive effect on petcoke conversion, as it would be expected according to previous batch results and established kinetic mechanism. Temperature increase has a positive and more pronounced effect on reduction capabilities of LY Mn ore, with respect to Ilmenite T1 and this is in agreement with literature results where manganese ore has slower reaction kinetics at lower temperatures with respect to ilmenite [25].

Steam content: An increase in water content helps petcoke gasification and expectedly has a positive effect on petcoke conversion. In the case of LY Mn ore, steam content is not a significant parameter for oxygen carrier conversion, contrary to ilmenite T1, which is highly sensitive to steam content in inlet gas to fuel reactor. This could be explained by looking more closely into experimental test conditions. Since the CO/CO2 ratio at the outlet of FR was a bit higher in the reference test case than at lower steam content, it means that more CO is produced in steam gasification reaction by increasing the H2O content, but not converted into CO2, so the consumption of oxygen carrier remains the same.

Petcoke flowrate: With LY Mn ore as an oxygen carrier, the effect of a petcoke flowrate increase on petcoke conversion is negligible, but it causes a higher oxygen carrier conversion for both materials. Indeed, more petcoke is sent to the fuel reactor, so the oxygen carrier needs to provide more oxygen to oxidize the petcoke gasification products. On the other hand, ilmenite shows clear positive increase for both reactivity indicators (R0ΔX and $X_{petcoke}$). When the petcoke flow rate increases, its conversion is slightly decreased and the oxygen carrier's conversion (R0ΔX) increases. Again, more petcoke is sent to the fuel reactor, so the oxygen carrier needs to provide more oxygen to oxidize the petcoke gasification products. At the same time, the petcoke conversion reduces due to decreased contact of gasification products with solids in the fluidized bed. This proves that LY Mn ore shows a lower potential for operation at high petcoke flowrate condition at an industrial scale in comparison to ilmenite.

Oxygen carrier flowrate: In the case of LY Mn ore test with an increased oxygen carrier flowrate, an increase in fuel conversion is observed which is contrary to what was observed with ilmenite. Fluidization gas flowrate and bed level in the fuel reactor remain the same, thus petcoke residence time in the fuel reactor should be the same as the oxygen carrier and consequently petcoke conversion should decrease. These different trends are not explained at the present time. An increase in oxygen carrier flowrate causes lower residence times of the solid in the fuel reactor, and expectedly, lower R0ΔX reduction values for both minerals.

Note that the target temperature of the fuel reactor temperature of the last test of

Table 10 was initially 930 °C but was not achieved during operation. Then, the influence of the oxygen carrier flowrate should have been more accentuated than what is shown by

Figure 8.

If petcoke and oxygen carrier residence times were independent, the impact of oxygen carrier flowrate on petcoke conversion should be negligible and petcoke conversion should be greatly impacted by petcoke flow rate. Actually, when the petcoke flowrate increases, its conversion is slightly decreased and the oxygen carrier R0ΔX increases (Figure 9 (c)). Indeed, more petcoke is sent to the fuel reactor, so the oxygen carrier needs to provide more oxygen to oxidize the petcoke gasification products. Furthermore, only a slight reduction of petcoke conversion is observed, which can be explained by the fact that petcoke is continuously being dragged away to the carbon stripper with the oxygen carrier. In that case, petcoke residence time is imposed by oxygen carrier residence time. Petcoke conversion is greatly impacted by oxygen carrier residence time (see

Figure 8(c)). When the oxygen carrier flowrate increases, its residence time decreases, as well as that of petcoke, hence petcoke conversion decreases as well.

Surprisingly, bed height does not impact petcoke conversion and oxygen carrier R0ΔX value. This is explained by a higher loss of petcoke dragged away with the fuel reactor gases (Figure 9(d)).

Overall, the conversion of petcoke achieved with LY Mn ore as an oxygen carrier is higher ($X_{petcoke}$ ≈85%) with respect to that obtained with Ilmenite T1 ($X_{petcoke}$≈70%).

Pilot plant operation highlighted certain issues with solid circulation as well as likely points of agglomeration. In particular, L-valves at FR outlet would see a certain solid build-up which quickly leads to pressure drop and prevent solids circulation. However, on process scale-up, larger diameters will be used for L-valves so fewer circulation issues are expected so long as the oxygen carrier flowrate is kept at high values (minimum 20 kg/h in 10 kWth pilot unit). To limit agglomeration issues, it is recommended to preheat the oxygen carrier to at least 850°C in the fluidization stage of unit start-up under oxidative atmosphere to ensure full oxidation condition. In addition, it is advisable to avoid hot points generation by progressively heating the unit from 400 to 900°C, while the solid is continuously fluidized with air or steam and circulated between reactors. In the unlikely case of stopping the solid circulation, it is advised to stop the fuel injection and maintain the solid fluidization while decreasing reactor temperature to around 700°C. By lowering the temperature, the operator could reduce the level of agglomeration of oxygen carrier in the reduced state (at FR outlet). Observed agglomeration behavior was the same for both oxygen carriers thus there are no specific recommendations for large scale operation at this time

Structural and morphological evolution of the oxygen carriers

LY Mn ore

This ore was obtained from China with the help of project partner Tsinghua University. The ore was calcined by the supplier at 1100°C for 8h, prior to crushing it to the requested particle size. A semi-quantitative X-ray fluorescence measurement shows that the ore contains mainly Mn and Fe as potentially redox active metals, as well as silicon, aluminum and other trace elements (Table 13).

X-ray Diffraction (XRD) analysis indicates that the fresh ore contains large amounts of tephroite (Mn2(SiO4)) and pyrolusite (MnO2) as well as some jacobsite (MnFe2O4) and some quartz (SiO2), along with other ill-defined and less abundant phases. Cross-section SEM analysis of the particles (Figure 10) shows the presence of highly crystalline precipitates in a matrix that contains dendrites which are usually formed during crystallization of metal alloys upon solidification. It is unclear whether this structure was initially present in the ore, or if it developed upon calcination. Lots of fine particles can also be seen despite the sieving that was performed to remove particles below 100µm.

Table 13: Semi-quantitative XRF analysis of the LY-Mn ore

Ca	***Fe***	***K***	***Mg***	***P***	***Si***	***Ti***	***Mn***	***Al***	***Ba***
0,14%	*7,28%*	*0,99%*	*0,26%*	*0,087%*	*9,46%*	*0,15%*	*47%*	*2,78%*	*0,81%*

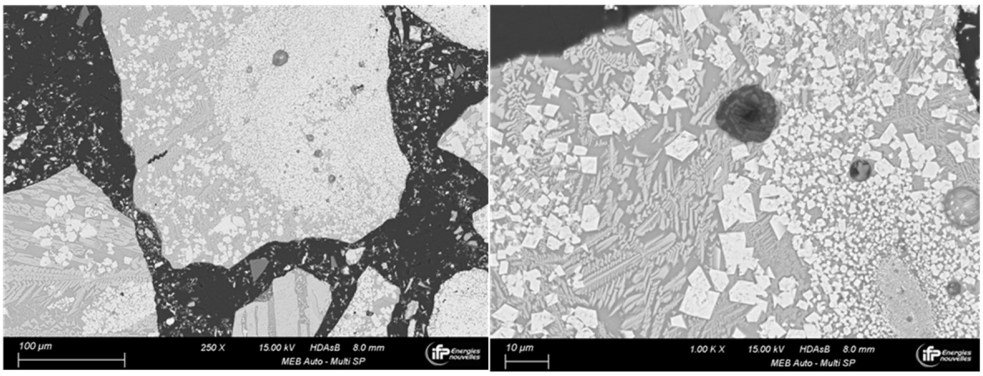

Figure 10: Cross-section SEM images of fresh LY-Mn ore

After methane activation, XRD analysis shows that most of the Mn and Fe are engaged in either hematite (Fe_2O_3) or bixbyite ($MnFeO_3$), along with some hausmannite (Mn_3O_4). The quartz initially present is still detected, as well as small amounts of pyroxmanganite ($(Mn,Fe)SiO_3$) and tephroite.

Direct SEM observation of the sample after activation shows the presence of what looks like an outgrowth of oxide(s), sometimes covering a large part of the surface of the particles, but mostly forming small, smooth looking 'islands' that are a few micrometers thick above the particles' surface (Figure 11).

Cross-section analysis of methane activated particles shows the same crystals and dendrites as the calcined ore, but some porosity can now be observed in some particles (Figure 12), which probably accounts for the activation of the ore. SEM observation of the particles after the complete test does not show much difference with the methane activated particles. However, when looking at the cross-section SEM analysis (Figure 13), it appears that while still present, both the crystallites and the dendrites inside the particles tend to give way to more porous particles, and XRD analysis indicates that most of the redox active metals have formed a $Mn_xFe_{1-x}O_3$ mixed oxide.

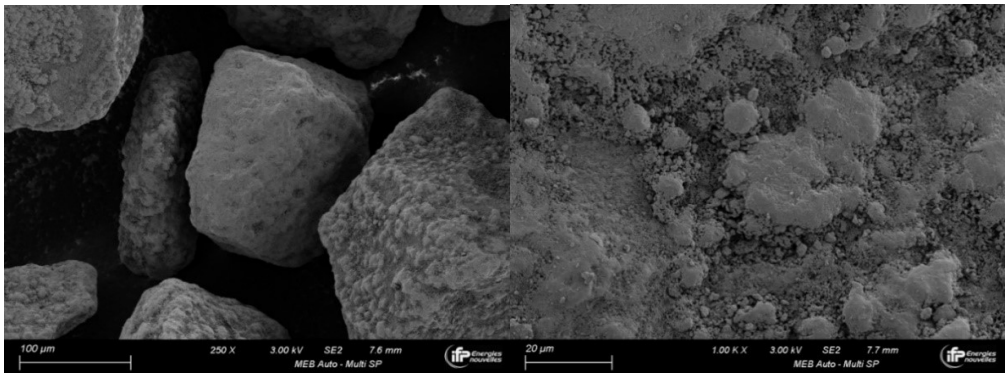

Figure 11: SEM images of LY-Mn ore powder after 52 hours of methane activation

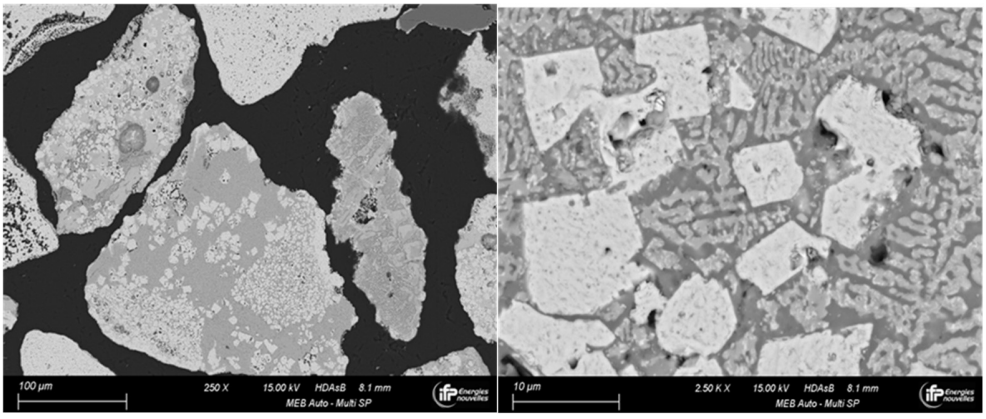

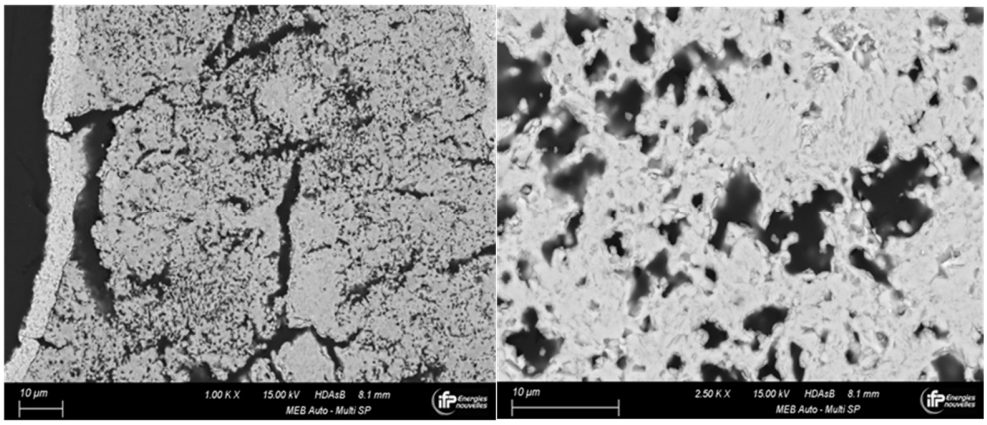

Figure 12: cross-section SEM images of LY-Mn ore powder after 52 hours of methane activation

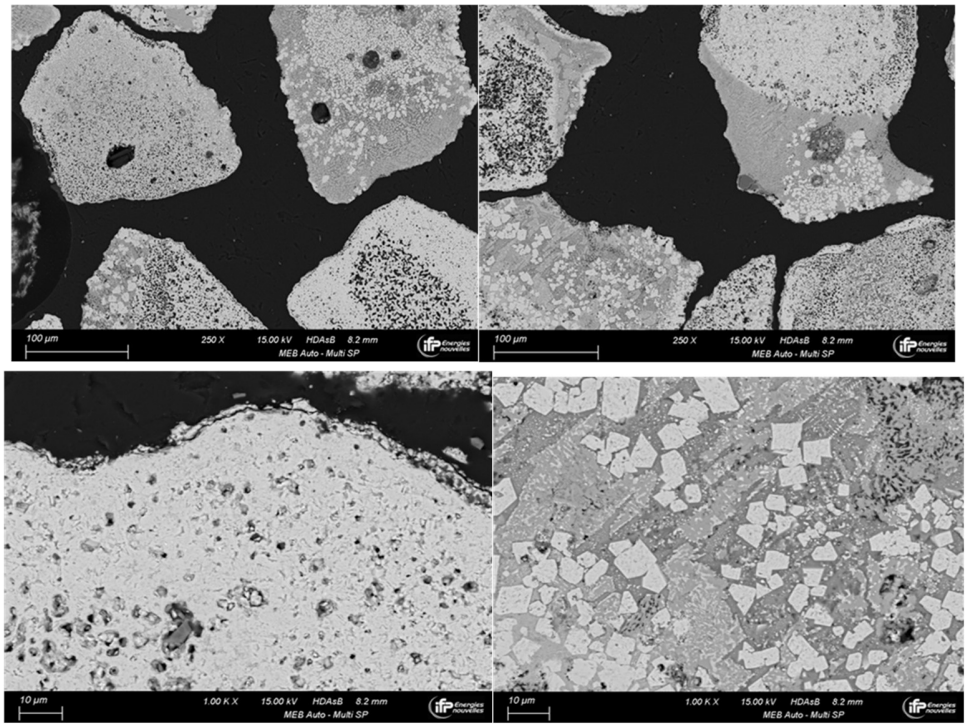

Figure 13: cross-section SEM images of LY-Mn ore powder after complete test

Ilmenite T1 ore

Ilmenite T1 ore was delivered by project partner SINTEF MK after sieving and drying, and was purchased from Titania AS, Norway. The main phases detected by XRD analysis are ilmenite ($FeTiO_3$) and hematite (Fe_2O_3). The main impurity detected is a silico-aluminate, possibly a disordered anorthite of formula $(Ca,Na)(Si,Al)_4O_8$ (see Table 14). SEM analysis shows that the particles present sharp edges, and that they are constituted of two main compositions (Figure 14): the brighter areas in the polished cross-section picture are constituted mainly of Fe and Ti oxides, while the darker areas are made of the alumino-silicate impurities.

Cross-section SEM analysis of the ilmenite particles over the activation period (Figure 15) shows that a layer of hematite (Fe_2O_3) is readily formed on the surface of the particles, and there is a gradual increase of porosity as well as formation of cracks. SEM-EDX (not shown) also shows that Fe an Ti progressively get segregated, as previously mentioned by [17]. Such a segregation is further confirmed by XRD analysis of the oxidized particles, where hematite (Fe_2O_3), titania (TiO_2) and

pseudo-brookite (Fe_2TiO_5) are the main detected phases after 108h activation, despite addition of fresh ilmenite halfway through methane activation.

Table 14 : Ilmenite T1 ore composition determined by semi-quantitative X-ray fluorescence measurement

TiO_2	Fe	MgO	SiO_2	Al_2O_3	CaO	Cr_2O_3	S	P_2O_5	Ni	Cu	Co
44.27	35.22	4.11	2.83	0.72	0.35	0.070	0.056	0.018	0.0165	0.0063	0.0111

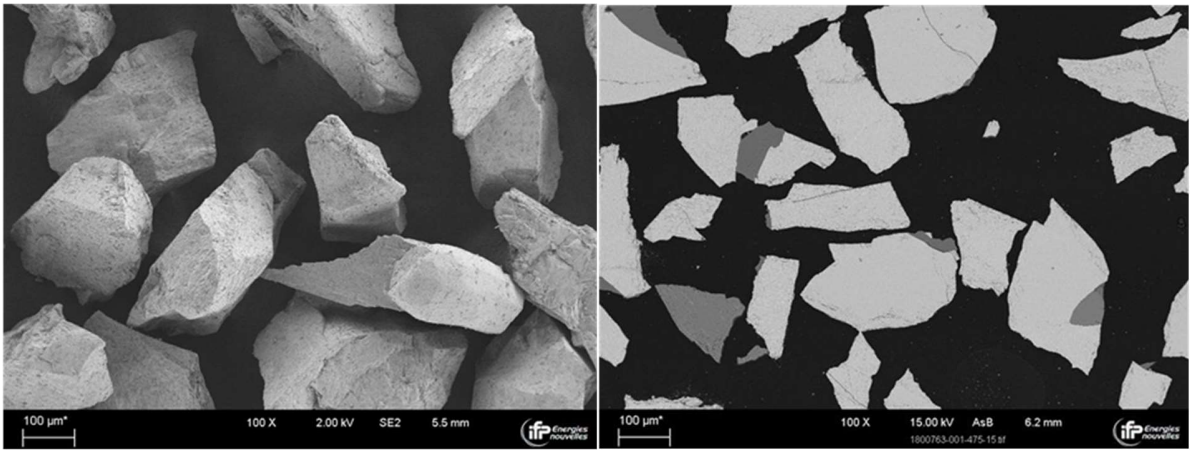

Figure 14: SEM images of ilmenite T1 (left: direct observation; right: polished cross-section)

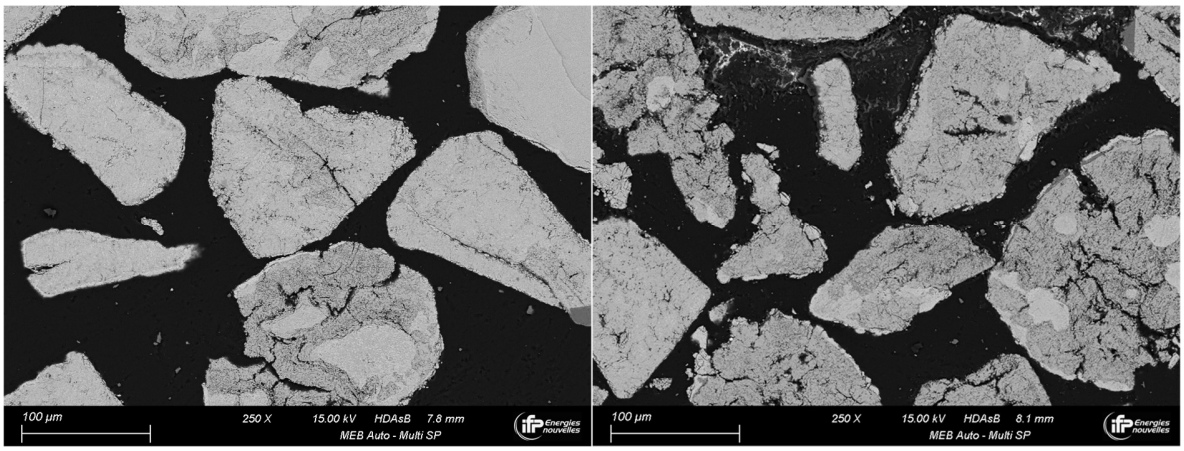

Figure 15: SEM cross-section analysis of Ilmenite during methane activation (left: after 34h; right: after 108h)

Very little phase and morphological evolution was observed after the petcoke tests compared to the activated particles. The nature of the fuel does not seem to have affected the behavior of the particles, but petcoke combustion was performed during a total of 23 hours only, after a total of 190h of methane exposition.

Lifetime of oxygen carriers

The fraction of fines produced is a good indicator of the mechanical resistance of the material.

Figure 16 shows the cumulated mass of fines recovered during the LY Mn campaign over the number of hours of circulation (612 h of total circulation and 65 h under combustible conversion). In total, 39 kg of OC were loaded in the unit and

7,3 kg of fines were produced, which represents a fine particles loss of 18.5 %.

The unit was initially filled with 31 kg of fresh OC distributed among the three reactors. Due to fluidization, a part of the solid continuously leaves at the gas outlet of the carbon stripper and at the cyclones. The accumulated OC was collected periodically at every outlet. A small part of this powder was kept as sample for analysis and the rest was sieved. Particles with a diameter higher than 100 µm were reintroduced in the pilot while the remaining particles (under 100 µm) were discarded. To avoid variations of gas and solid residence time in the fuel reactor, the operating conditions have been chosen to maintain a constant solid level in the fuel reactor during the entire campaign duration (except if specifically mentioned).

Switching from gas to solid fuel injection does not drastically change the fines formation, as can be seen in Figure 16. The mean value of inventory loss under methane exposure is 0.30%/h (or 0.12 kg/h) which leads to a particle lifetime of approximately 331 hours. With petcoke, the inventory loss is around is 0.21%/h, leading to a particle lifetime of 482 h.

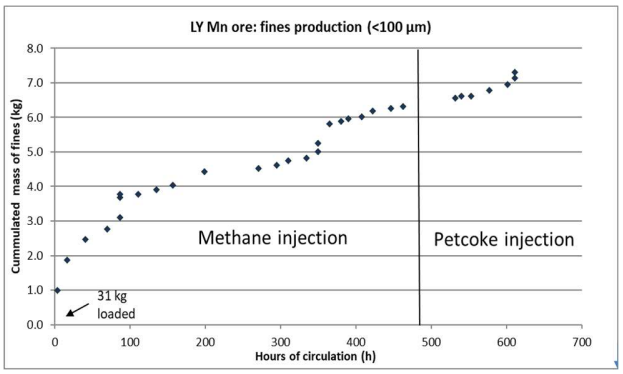

Figure 16: Mass of fines recovered as a function of circulation time during LY Mn campaign (Petcoke combustion was not performed on a continuous basis).

Figure 17 shows the amount of fine particles recovered in the cyclones and filter candles as a function of ilmenite circulation time, as well as the amounts and times of fresh ilmenite addition throughout the ilmenite campaign. No fines were collected after the start-up procedure (the candles were not cleaned during the first 100 hours circulation, and no particles below 100µm were collected from the cyclones), which implies that fresh particles are mechanically strong and well suited for fluidization. However, after methane activation started, the amount of collected fines increases somehow linearly with the particles' circulation time, and the change to petcoke combustion reduced slightly the fines' formation rate. The mean value of inventory loss calculated under methane exposure is 0,13%/h, leading to a particle lifetime of 770h. When petcoke is used as fuel, the inventory loss is around 0.07%, which corresponds to a particle lifetime of 1430h. These differences of fines production rate can be explained by the difference of mean $R_0\Delta X$ value (0.85% against 0.60%) observed during methane and petcoke tests.

The estimated lifetimes of both oxygen carriers are in line with some previous experiments in the Chalmers 10 kW CLC unit which have shown that manganese ores are more sensitive to attrition than ilmenite, with respective lifetimes of 50-290 hours [3, 12, 28] and 700-800 hours [29].

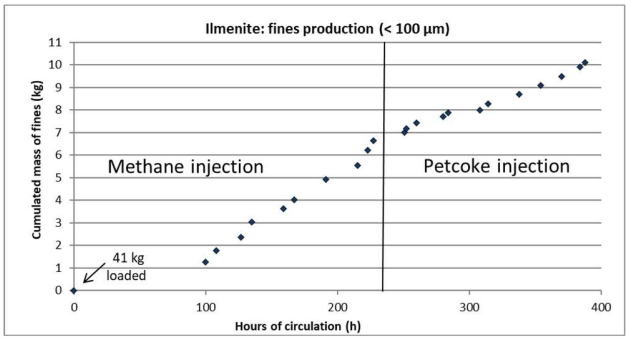

Figure 17: Mass of fines recovered as a function of circulation time during ilmenite campaign (Petcoke combustion was not performed on a continuous basis)

Conclusion

Chemical Looping Combustion (CLC) is a promising CCUS technology for combustion processes that could achieve high efficiencies for power, steam and heat generation. In the scope of the CHEERS project, two different oxygen carriers were characterized and tested in a continuous pilot unit of 10 kW_{th} capacity.

In IFPEN's 10 kW_{th} pilot unit with high solid residence time and with LY Mn ore as oxygen carrier, a petcoke conversion of up to 89% was observed without any recycle of unburnt petcoke. The reactivity of LY Mn ore is high enough to convert the gases produced by petcoke gasification. Where the reduction potential of oxygen carrier is concerned, it was observed that LY Mn ore has a high initial $R_0\Delta X$ value ($R_0\Delta X$=0.8), which lead to shorter activation period in comparison to Ilmenite T1 which required a longer activation period to reach its full potential. This is in accordance with a study that was done at Tsinghua University [21] which suggests that oxygen carrier conversion is higher for manganese ore than for ilmenite. Overall, both oxygen carriers have different performances: LY Mn global conversion with petcoke as fuel is better than ilmenite whereas the latter converts methane better. Furthermore, with LY Mn as oxygen carrier, the mean value of inventory loss under methane exposure is 0.30%/h (or 0.12 kg/h) which leads to a particle lifetime of approximately 331 hours. With petcoke, the inventory loss is around is 0.21%/h, leading to a particle lifetime of 482 h. Fragmentation of LY Mn ore seems to be more important with methane as fuel. As a comparison, for ilmenite, the mean value of inventory loss calculated under methane exposure is 0,13%/h, leading to a particle lifetime of

770 h. When petcoke is used as fuel, the inventory loss is around 0.07%, which corresponds to a particle lifetime of 1430 h. This shows that LY Mn ore is more sensitive to attrition than ilmenite, under similar operating conditions, which is a critical characteristic for large scale deployment. Lifetimes of OCs is integrated in techno-economic studies to select the most suitable OCs. In particular, lifetime of ilmenite is sufficiently high for large scale operation. For commercial unit operation, it is expected to further improve the material lifetime by using synthetic materials. Production cost of ilmenite (100 $/ton) has been reported cheaper than manganese ores (200-300$/ton) [20] in the recent years, which is an important parameter for large scale unit design, given the high OC turnover that is expected in operation with solid fuels.

Agglomeration issues are expected to occur in the demonstration unit but with less impact than in smaller units since lines diameter will be larger in the demonstration unit. Furthermore, it is recommended to add aeration in the lines to limit the non-fluidized zones. The key manipulable variables for continuous operation that could be applied in large scale operation of demonstration unit were identified as following:

• **Fuel reactor temperature** significantly increases solid fuel conversion and oxygen transfer capacity of the oxygen carrier.

• **Oxygen carrier flowrate** affects $R_0\Delta X$ value significantly since it determines the residence time of oxygen carrier in the reactor

• **Petcoke flowrate** has a significant effect on the reduction potential of oxygen carrier in the fuel reactor, whereby it is possible to double the $R_0\Delta X$ value by adjusting the petcoke flowrate. This means that it is possible to operate at high $R_0\Delta X$ values at large scale.

Table 15 Overview of KPIs for selection of OC for demonstration unit operation

Parameter	*Ilmenite*	*LY Mn ore*
CH4 conversion	+	-
Petcoke conversion	-	+
$\frac{CO}{CO_2}$ *at FR outlet*	+	-
Lifetime	+	-
Production cost	+	-

In order to make the final selection for the best suited candidate for operation of world's largest demonstration unit of CLC technology, key performance indicators were taken into account (Table 15) and overall Ilmenite seems to be a better candidate than LY Mn since attrition sensitivity and production cost are lower, even if performances towards solid fuel conversion are better with LY Mn. It is expected that with experimental data and operational experience of this unit, significant advances in CLC technology commercialization will be made.

AUTHOR INFORMATION

Corresponding Authors

Nicolas VIN: nicolas.vin@ifpen.fr

ACKNOWLEDGMENT

This work has received funding from the European Union's Horizon 2020 research and innovation program under grant agreement No 764697. The CHEERS project is also co-funded from National Key Research and Development Program of China by Chinese Ministry of Science and Technology (MOST) under grant agreement No 2017YFE0112500.

ABBREVIATIONS

CLC: Chemical Looping Combustion

CCS: Carbon capture and Storage

CHEERS: Chinese-European Emission-Reducing Solutions

OCs: Oxygen carriers

AR1: Air reactor 1

AR2: Air Reactor 2

CS: Carbon Stripper

FR: Fuel Reactor

REFERENCES

1. Nandy A, Loha C, Gu S et al. (2016) Present status and overview of Chemical Looping Combustion technology. Renewable and Sustainable Energy Reviews 59:597–619. https://doi.org/10.1016/j.rser.2016.01.003
2. Lyngfelt A, Linderholm C (2017) Chemical-Looping Combustion of Solid Fuels – Status and Recent Progress. Energy Procedia 114:371–386. https://doi.org/10.1016/j.egypro.2017.03.1179
3. Linderholm C, Lyngfelt A, Cuadrat A et al. (2012) CLC of solid fuels – 10kW unit with two fuels, above-bed and in-bed fuel feed and two oxygen carriers, manganese ore and ilmenite. Fuel 102:808–822. https://doi.org/10.1016/j.fuel.2012.05.010
4. Markström P, Linderholm C, Lyngfelt A (2013) Chemical-looping combustion of solid fuels – Design and operation of a 100kW unit with bituminous coal. International Journal of Greenhouse Gas Control 15:150–162. https://doi.org/10.1016/j.ijggc.2013.01.048
5. Schmitz M, Linderholm C, Hallberg P et al. (2016) Chemical-Looping Combustion of Solid Fuels Using Manganese Ores as Oxygen Carriers. Energy Fuels 30:1204-1216. https://doi.org/10.1021/acs.energyfuels.5b02440
6. Lyngfelt A (2020) Chemical Looping Combustion: Status and Development Challenges. Energy Fuels 34:9077–9093. https://doi.org/10.1021/acs.energyfuels.0c01454
7. Johansson Marcus, Matisson Tobias and Lyngfelt Anders Comparison of oxyden carriers for chemical-looping combustion
8. Lyngfelt A, Brink A, Langørgen Ø et al. (2019) 11,000 h of chemical-looping combustion operation—Where are we and

where do we want to go? International Journal of Greenhouse Gas Control 88:38–56. https://doi.org/10.1016/j.ijggc.2019.05.023
9. Abad A, Gayán P, Pérez-Vega R et al. (2020) Evaluation of different strategies to improve the efficiency of coal conversion in a 50 kWth Chemical Looping combustion unit. Fuel 271:117514. https://doi.org/10.1016/j.fuel.2020.117514
10. Cuadrat A, Abad A, García-Labiano F et al. (2012) Relevance of the coal rank on the performance of the in situ gasification chemical-looping combustion. Chemical Engineering Journal 195-196:91–102. https://doi.org/10.1016/j.cej.2012.04.052
11. Pérez-Vega R, Abad A, García-Labiano F et al. (2016) Coal combustion in a 50kWth Chemical Looping Combustion unit: Seeking operating conditions to maximize CO2 capture and combustion efficiency. International Journal of Greenhouse Gas Control 50:80–92. https://doi.org/10.1016/j.ijggc.2016.04.006
12. Linderholm C, Lyngfelt A, Dueso C (2013) Chemical-looping combustion of solid fuels in a 10kW natural minerals as oxygen carrier. Energy Procedia 37:598–607. https://doi.org/10.1016/j.egypro.2013.05.147
13. Thon A, Kramp M, Hartge E-U et al. (2014) Operational experience with a system of coupled fluidized beds for chemical looping combustion of solid fuels using ilmenite as oxygen carrier. Applied Energy 118:309–317. https://doi.org/10.1016/j.apenergy.2013.11.023
14. Ströhle J, Orth M, Epple B (2015) Chemical looping combustion of hard coal in a 1 MWth pilot plant using ilmenite as oxygen carrier. Applied Energy 157:288–294. https://doi.org/10.1016/j.apenergy.2015.06.035
15. Qasim M, Ayoub M, Ghazali NA et al. (2021) Recent Advances and Development of Various Oxygen Carriers for the Chemical Looping Combustion Process: A Review. Ind Eng Chem Res 60:8621–8641. https://doi.org/10.1021/acs.iecr.1c01111
16. Mei D, Mendiara T, Abad A et al. (2016) Manganese Minerals as Oxygen Carriers for Chemical Looping Combustion of Coal. Ind Eng Chem Res 55:6539–6546. https://doi.org/10.1021/acs.iecr.6b00263
17. Matzen M, Pinkerton J, Wang X et al. (2017) Use of natural ores as oxygen carriers in chemical looping combustion: A review. International Journal of Greenhouse Gas Control 65:1–14. https://doi.org/10.1016/j.ijggc.2017.08.008
18. Abad A, Gayán P, Mendiara T et al. (2018) Assessment of the improvement of chemical looping combustion of coal by using a manganese ore as oxygen carrier. Fuel Processing Technology 176:107–118. https://doi.org/10.1016/j.fuproc.2018.03.026
19. Arjmand M, Leion H, Mattisson T et al. (2014) Investigation of different manganese ores as oxygen carriers in chemical-looping combustion (CLC) for solid fuels. Applied Energy 113:1883–1894. https://doi.org/10.1016/j.apenergy.2013.06.015
20. Arjmand M, Leion H, Lyngfelt A et al. (2012) Use of manganese ore in chemical-looping combustion (CLC)—Effect on steam gasification. International Journal of Greenhouse Gas Control 8:56–60. https://doi.org/10.1016/j.ijggc.2012.02.001
21. Chen H, Li Z, Wang R (2021) Design Theory of a CLC Air Reactor with Oxygen Carrier Recirculation and Its Application to a 3 MW th Pilot. Energy Fuels 35:1580–1593. https://doi.org/10.1021/acs.energyfuels.0c03111
22. Sundqvist S, Khalilian N, Leion H et al. (2017) Manganese ores as oxygen carriers for chemical-looping combustion (CLC) and chemical-looping with oxygen uncoupling (CLOU). Journal of Environmental Chemical Engineering 5:2552–2563. https://doi.org/10.1016/j.jece.2017.05.007
23. Sundqvist S, Arjmand M, Mattisson T et al. (2015) Screening of different manganese ores for chemical-looping combustion (CLC) and chemical-looping with oxygen uncoupling (CLOU). International Journal of Greenhouse Gas Control 43:179–188. https://doi.org/10.1016/j.ijggc.2015.10.027
24. Sundqvist S, Mattisson T, Leion H et al. (2018) Oxygen release from manganese ores relevant for chemical looping with oxygen uncoupling conditions. Fuel 232:693–703. https://doi.org/10.1016/j.fuel.2018.06.024
25. Kajnäs C, Hedberg M, Leion H (2019) The Effect of Iron- and Manganese-Based Oxygen Carriers as Bed Materials in Oxygen Carrier Aided Combustion. Energy Technol 7:1900321. https://doi.org/10.1002/ente.201900321
26. Liu L, Li Z, Li W et al. (2019) The melting characteristics of Vietnamese ilmenite and manganese ores used in chemical looping combustion. International Journal of Greenhouse Gas Control 90:102792. https://doi.org/10.1016/j.ijggc.2019.102792
27. Larring Y, Braley C, Pishahang M et al. (2015) Evaluation of a Mixed Fe–Mn Oxide System for Chemical Looping Combustion. Energy Fuels 29:3438–3445. https://doi.org/10.1021/acs.energyfuels.5b00048
28. Linderholm C, Schmitz M, Knutsson P et al. (2016) Chemical-looping combustion in a 100-kW unit using a mixture of ilmenite and manganese ore as oxygen carrier. Fuel 166:533–542. https://doi.org/10.1016/j.fuel.2015.11.015
29. Linderholm C, Knutsson P, Schmitz M et al. (2014) Material balances of carbon, sulfur, nitrogen and ilmenite in a 100kW CLC reactor system. International Journal of Greenhouse Gas Control 27:188–202. https://doi.org/10.1016/j.ijggc.2014.05.001

TOC graphic